Mechanical Systems and Signal Processing 138 (2020) 106548

Contents lists available at ScienceDirect

Mechanical Systems and Signal Processing

journal homepage: www.elsevier.com/locate/ymssp

Model predictive control of three-axis gimbal system mounted on UAV for real-time target tracking under external disturbances

Aytaç Altan *, Rıfat Hacıoğlu

Department of Electrical Electronics Engineering, Zonguldak Bülent Ecevit University, 67100 Zonguldak, Turkey

ARTICLE INFO

Article history:
Received 31 May 2019
Received in revised form 22 November 2019
Accepted 30 November 2019
Available online 3 January 2020

Keywords:
UAV
Gimbal system
Hammerstein
Model predictive control
Target tracking

ABSTRACT

The fact that Unmanned Aerial Vehicles (UAVs) move in a specific path and that the camera in the gimbal system mounted on the UAV adhere to the right target attracts the attention of many researchers. The effective control of the gimbal system directly affects the performance of the UAV which is tracking a predetermined moving target, following a specified path. The contribution of this study is not only modelling three-axis gimbal system mounted on mobile platform based on nonlinear Hammerstein block structure to control effectively using model predictive controller (MPC) but also improving real time target tracking performance under external disturbances. A novel Hammerstein model based MPC controller is successfully proposed for real time target tracking of three-axis gimbal system applying flight scenarios of UAV to be robust under external disturbances. In this study, firstly, the mathematical model of three-axis gimbal system mounted on UAV is developed based on traditional Newton–Euler method. Secondly, linear and nonlinear modeling based on the input and output data of the three-axis gimbal system mounted on UAV moving autonomously for target tracking is emphasized. The linear output error (OE) and nonlinear block structure Hammerstein models of the three-axis gimbal system are identified under the external disturbance effect, respectively. Then, the identified Hammerstein model is embedded in the flight control card, which included the three-axis gimbal system control to realize real time target tracking of the UAV. Afterwards, the MPC of three-axis gimbal system is realized under the external disturbance with linear and nonlinear models. Also, the performance of proposed MPC controller with Hammerstein model is evaluated comparing with conventional PID controller in terms of robustness and quantitative study of error analysis. Finally, the stability and robustness of the three-axis gimbal system controlled with the MPC algorithm has been investigated by the test results carried out in different scenarios. The simulation and experimental results show that the proposed MPC algorithm with Hammerstein model in this paper can ensure that the UAV exactly tracking the target while maintaining stability, even with external disturbances.

* Corresponding author.
E-mail address: aytacaltan@beun.edu.tr (A. Altan).

https://doi.org/10.1016/j.ymssp.2019.106548
0888-3270/

1. Introduction

Unmanned aerial vehicles (UAVs), which are frequently used in defense industry with civil and academic studies are used in many different tasks such as mapping, search and rescue, payload transportation, exploration and surveillance, inspection, border security and instant image transferring from the air by following the target [1,2]. The UAVs, which can act autonomously according to military and civilian missions, are designed with various equipment such as global positioning system (GPS), camera gimbal system, load transporting system (LTS), vertical take-off and landing (VTOL) system, flight control, image transfer, telemetry and laser marking modules [3,4]. It is known that the camera gimbal system, which is among these equipment on the UAVs, plays an important role in tracking the target with minimum error by following a specified path [5,6]. In UAVs, the gimbal system has been widely used in recent years to stabilize the observation system with optical equipment such as camera, radar and laser, or the platform equipped with different measuring devices. The stabilization algorithm of the gimbal system is basically based on a regulator with a feedback loop [7]. Thanks to the stabilization platform called gimbal system on the UAV, more sensitive measurements can be made with measuring devices such as laser, camera and inertial measurement unit (IMU) sensor attached to the platform. Thus, the probability that the obtained data or information is affected by external disturbances is minimized [8]. In this paper, a model predictive control (MPC) approach based on the nonlinear Hammerstein model has been proposed for the three-axis gimbal system mounted on UAV used in target tracking to be robust under external disturbance.

The control algorithms of both UAV and gimbal systems at the same time are described as a complex engineering problem. In many applications, UAV and gimbal mounted on UAV are controlled separately by different control algorithms [9,10]. Gimbal systems are designed to point and stabilize about two or more axes, and for this reason, at least two orthogonal gimbals are required in most applications such as cameras, weapon systems, laser sensors and telescopes. In order to provide additional degrees of freedom or to obtain better isolation from the UAV, it is often necessary to have more than two gimbals [11]. In this study, a three-axis gimbal system is used to expand the workspace, to track precisely and accurately the target and to hold a line of sight (LOS) stationary. In the real-time target tracking, the novel control algorithm proposed for the control of the three-axis gimbal system is integrated into the UAV by being embedded in the flight control card on the UAV.

The control of such gimbal systems mounted on UAV is not a simple problem to maintain stable operation and guarantee accurate positioning and tracking of the sensor for the target due to the system dynamics and operating conditions change [12]. In recent years, studies on the model and control of gimbal system mounted on UAV have been frequently included in the literature. In [12], the sensor on the two axes gimbal system has been isolated from external disturbances induced by the operating environment and a self-tuning proportional-integral-derivative (PID) type fuzzy controller has been suggested to stabilize the line of sight to the target. The overall control system is modeled by considering the inertia cross-coupling and the stabilization loops are formed with the cross-coupling unit using the proposed fuzzy PID controller. In [13], a control scheme based on the slide mode control technique for two axes gimbal system has been designed. It is noted that good tracking is provided by the sliding mode controller, which is designed against unknown disturbances and system parameters. Also, a linear quadratic Gaussian (LQG) algorithm based on a simple first-order linear stochastic differential equation is presented in order to estimate and compensate for real time a particular class of disturbances. In [14], a vision-based neuro-fuzzy controller is designed for a two-axis gimbal system mounted on a small UAV. In the designed controller unit, vision-based object detection has been used as an input and an algorithm has been developed to generate pan and tilt motion and velocity commands for the gimbal in order to keep the interest object at the center of the image frame. Also, a learning algorithm that addresses the dynamic and nonlinear characteristics of the gimbal movement has been developed for a radial basis function based neuro-fuzzy system and controller. Besides conventional control methods [15], some advanced control techniques such as fuzzy control [12,14], robust control [16], variable structure control [17], H_∞ control methodology [18], and neural networks control [19,20] have been applied in LOS inertia stabilization systems (ISP). The variable structure-augmented adaptive controller which is applied to a gyro-mirror line-of-sight stabilization platform has been proposed [17]. In [18], the H_∞ control methodology has been used to design a high performance controller as to control the rate of the line of sight. The LOS stabilization control based on gyro stabilized platform is required to isolate the LOS from the disturbance and vibration of carrier and ensure pointing and tracking for target in electro optical tracking system [21].

Fuzzy logic technique, which is a powerful tool for dealing with the control of nonlinear system models, is frequently used. The control problems such as high stabilization sensitivity for nonlinear uncertainty servo system [21], reliable tracking control for near-space hypersonic vehicle exposed to aperiodic measurement information [22], and trajectory tracking for unmanned vehicles are often carried out by fuzzy logic technique [23]. In [23], real-time tracking of reference trajectory with various geometries has been performed by the UAV which is acting autonomously with the self-tuning fuzzy PID controller. The proposed fuzzy PID controller for trajectory tracking has been compared with conventional PID according to maximum and total error performances. It has been determined that the maximum and total error performance of the UAV improved between forty-three percent and fifty-seven percent with fuzzy PID controller according to conventional PID controller.

The model-based studies for target tracking seem to be focused on the control of the UAV rather than gimbal's control. The effective control not only of the UAV, but also of the gimbal, plays an important role in terms of performance of the target tracking task. In [24], it has been focused on the design and implementation of a new search and track payload system that uses an MPC that includes the design of the controller responsible for directing the UAV to its interests and the optimal

gimbal orientation for placing objects of interest in the image center of the camera. In [25], the performance of the gimbal system testing one axis gimbal system in consideration of the flight dynamics and the 6-DOF motion equations is evaluated to estimate the total uncertainty. In the literature, there are studies on model based control using the mathematical model of the gimbal system fixed on a non-moving platform. On the other hand, in this study, the three-axis gimbal system that is mounted on the UAV is on moving platform. The parameter complexity of the identified Hammerstein model, which performs well against external disturbances caused both moving platform and environmental conditions, is minimized and the control mechanism of the three-axis gimbal system is tried to be optimized.

Neural networks can effectively deal with non-linear disturbance in the system for their universal approach capability, but suffer training time and data length to optimize model structure [26]. Although the fuzzy logic technique is a powerful tool for dealing with the control of non-linear system models, significant changes in the system's control performance may occur due to non-linear internal and external disturbances in the system [27]. When this technique is used in conjunction with the PID controller, it is necessary to recalculate the controller coefficients in load changes. This situation can adversely affect the control performance of the system in real-time applications. The control performance of the three-axis gimbal system for real-time applications can be improved by using the nonlinear model which is identified as robust against the sudden load changes. This model can be used in MPC with minimum parameter complexity. The main contribution of this study is to perform the control of the three-axis gimbal system which has nonlinear structure mounted on the UAV, which is a moving platform, with the Hammerstein model, which has minimum parameter complexity and the robust against external disturbances. Thus, it is ensured that both maximum and total error amount of UAV are minimized for real time target tracking.

In this paper, not only the mathematical model, but also robust linear and nonlinear models of the three-axis gimbal have been obtained under external disturbance. Both the model and the controller are designed to be robust under external disturbance for the high performance of the novel MPC controller with the Hammerstein model which is proposed for the three-axis gimbal used in target tracking. The remainder of this paper is organized as follows. Target tracking problem is defined in Section 2 and the mathematical model of a three axis gimbal system mounted on UAV is obtained by deriving gimbal motion equations in Section 3. Identification of the linear output error (OE) and nonlinear Hammerstein models of the three-axis gimbal system under the external disturbance are defined in Section 4. Afterwards, in Section 5 the MPC controller for OE and Hammerstein models are designed to compensate for disturbances and uncertainties of the three-axis gimbal system. Then, the MPC controller with individually identified OE and Hammerstein models of three-axis gimbal system is realized for real time target tracking of the UAV under the external disturbance and the experimental results are introduced in Section 6. Finally, the conclusion remarks are highlighted in Section 7.

2. Problem definition for target tracking

The gimbal on which a gyroscope or set of gyroscopes are mounted consists of bearings and motors. The gimbals are used to stabilize cameras, sensors, weapon systems and telescopes used for civil and military purposes. The sensor system or payload to be stabilized can be mounted directly on the gimbal assembly. In some configurations, however, mirrors or other optical elements are mounted to the gimbal and the sensor is fixed to the UAV. Although the requirements for the gimbals vary widely depending on the application, it is a common goal of all of them to keep or control the LOS of one object according to another object or inertial space [11]. The LOS orientation is determined by the angular displacements of the gimbal assemblies. When the UAV is maneuvering or vibrating, a properly operating gimbal rotates in the opposite direction, ensuring that the LOS orientation is remained stable relative to the inertial space. For this reason, the gimbal movement directly determines the LOS direction and image vibration [28]. The three-axis gimbal platform generally comprises a motor for driving each axis, position sensors for measuring the angle and a gyroscope for measuring the speed of the gimbal. The stabilization of the three-axis gimbal system used in this study is achieved by suspending the camera placed on the end effector of the three-axis gimbal system shown in Fig. 1. The three-axis gimbal system is consisted of three revolute joints and it has been represented yaw-roll-pitch axis.

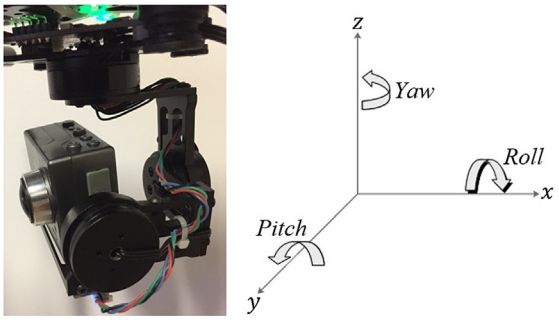

Fig. 1. Three-axis gimbal system mounted on UAV.

The gyroscope outputs are used as feedback to torque motors associated with gimbals to provide alignment error tracking and stabilization against base angular motion. The control system of the three-axis gimbal system mounted on UAV tries to align with the LOS line, which connects the camera axis with the target as shown in Fig. 2 so that the camera axis is kept nonrotating in an inertial space despite torque disturbances. Therefore, the stabilization loop must isolate the camera from the angular base motion and external disturbances that disturb the target point [12]. Although there are many approaches are available to stabilizing the LOS of an object so that it doesn't rotate according to inertial space, perhaps the clearest and most common approach is mass stabilization. The principle of mass stabilization is essentially an acknowledgment of Newton's first and second laws of motion. According to Newton's first and second laws, all that is required to prevent an object from rotating with respect to inertial space is to ensure that the applied torque is zero. However, notwithstanding careful electromechanical design, numerous sources of torque disturbances can act on a real mechanism causing excessive movement or jitter of the LOS. Therefore, rate or displacement gyroscopes are typically attached to the object to measure the inertial rotation about the axes that require stabilization and control [11]. In Fig. 2, the camera frame is relative to the gimbal and the angle between the target and pointing direction of the camera Z_c is denoted $\mathcal{E}$. The target tracking performance is determined by minimizing the $\mathcal{E}$ angle between the target and the pointing direction of the camera Z_c mounted on the gimbal system on the UAV.

The problems with undesirable overshoot, longer settling times, vibrations and stability are also present for the three-axis gimbal control system, and dealing with these problems are crucial. To deal with these problems, the control structure of the three-axis gimbal system will be realized using the MPC controller. Each control loop in the three axes of the gimbal system is concerned the cross coupling unit formed based on the relationships of the torques. Each joint has an effect on other joints. The characteristics of the dynamic of the gimbal system are expressed by cross coupling. In this paper, both mathematical model considering the dynamic mass unbalance and robust linear and nonlinear models for MPC control of the three-axis gimbal system are obtained under external disturbance. Here we assume that the external disturbance is random variable and bounded. Not only the model but also the controller have been designed and tested to be robust against to external disturbance for the high performance of the novel MPC controller with the Hammerstein model proposed for the three-axis gimbal system mounted on the autonomously moving UAV used in real time target tracking.

3. Mathematical modeling of gimbal system

This section details the mathematical model of a three-axis gimbal system depicted in Fig. 1 for target tracking. The three-axis gimbal system is mounted under a UAV as shown in Fig. 2 and the rotation of each motor of the gimbal is limited to avoid any mechanical shock. It is very important to obtain an appropriate dynamic model for effective control of the gimbal system mounted on the UAV. In the control process, the dynamic model of the gimbal system tries to produce the appropriate torque value to ensure the desired system response and performance.

Definition 1. The nonlinear dynamic equation of the gimbal system for angular position vector θ is defined as

$$M(\theta)\ddot{\theta} + V\left(\theta, \dot{\theta}\right) + F\left(\dot{\theta}\right) + G(\theta) + \tau_d = \tau \tag{1}$$

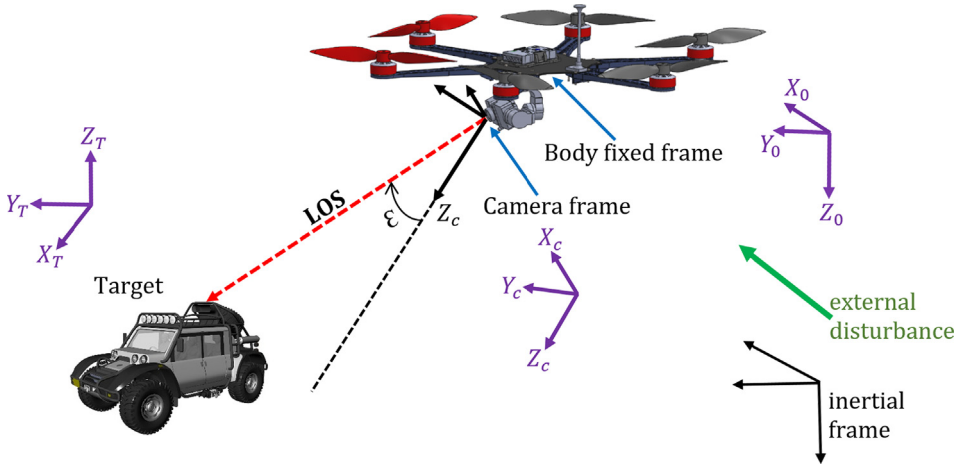

Fig. 2. Schematic diagram of three-axis gimbal system mounted on UAV for target tracking.

where τ is force vector for each axis, $M(\theta)$ is inertia matrix, $V\left(\theta,\dot{\theta}\right)$ is coriolis/centripetal vector, $F\left(\dot{\theta}\right)$ is friction term consisting of dynamic and viscous friction, $G(\theta)$ is gravity vector and τ_d is external disturbance term. This term is an 3×1 vector that represents an additive disturbance for three-axis gimbal system.

Definition 2. *The gimbal dynamics in the conservation of energy form is*

$$\frac{1}{2}\frac{d}{dt}\left[\dot{\theta}^T M(\theta)\dot{\theta}\right] = \dot{\theta}^T\left[\tau - G(\theta) - F\left(\dot{\theta}\right)\right] \tag{2}$$

where the left-hand side of Eq. (2) is the derivative of the gimbal kinetic energy, and the right-hand side of Eq. (2) represents the power supplied from the actuators difference of the power dissipated due to gravity and friction. Note that the coriolis/-centripetal terms are accounted in Eq. (2) since these terms are related to the time derivative of the inertia matrix. The conservation of energy formulation given in Eq. (2) is exploited to design an adaptive controller in the target tracking problem.

Since we design an adaptive controller for target tracking, a Lyapunov function is selected, which is a function of the tracking error and the parameter error. The inertia related Lyapunov-like function is defined as

$$V = \frac{1}{2}\left[r^T M(\theta)^r + \widetilde{\varphi}^T\Gamma^{-1}\,\widetilde{\varphi}\right] \tag{3}$$

where $r = \Lambda e + \dot{e}$, $\varphi = \varphi - \widehat{\varphi}$ and $\Gamma = diag(\gamma_1, \gamma_2, \cdots, \gamma_r)$. Here, γ_i's are positive scalar constants for $i = 1, \cdots, r$ and Λ is defined as positive-definite, diagonal matrix such that $\Lambda = diag(\lambda_1, \lambda_2, \cdots, \lambda_r)$. Specifically, with the addition of the bounded disturbance term in Eq. (1), the derivative of the Lyapunov-like function is

$$\dot{V} = -r^T K_v r + r^T\tau_d \tag{4}$$

By using of the Rayleigh-Ritz method, Eq. (4) can be expressed as

$$\dot{V} \le -\lambda_{min}\{K_v\}\|r\|^2 + \|r\|\|\tau_d\| \tag{5}$$

A sufficient condition on the negativity of $\dot{V}$ can be obtained from Eq. (5). That is, $\dot{V}$ will be negative if

$$\|r\| > \frac{\|\tau_d\|}{\lambda_{min}\{K_v\}} \tag{6}$$

If Eq. (6) is satisfied, $\dot{V}$ is nagative and V will decrease. If V decreases, then by our definition on the Lyapunov-like function given in Eq. (3), r must eventually decrease. However, if r decreases such that

$$\|r\| \le \frac{\|\tau_d\|}{\lambda_{min}\{K_v\}} \tag{7}$$

then $\dot{V}$ may become positive, which means that V will start to increase. If V starts to increase, we gain insight into the problem by examining two possibilities. One, the increase in V causes r to increase such that Eq. (6) is satisfied. The other possibility is that the increase in V causes $\widetilde{\varphi}$ to increase while r stays small enough such that Eq. (7) is satisfied.

The kinematic model of the three-axis gimbal mechanism is helped to identify the gimbal workspace and to control of the end effector position. The gimbal used in the study consists of three revolute joints and is represented by the yaw-roll-pitch axis. Also, the yaw-roll-pitch angles of the three axis gimbal are expressed by θ_1, θ_2 and θ_3 respectively. An orthogonal coordinate system that rotates with each member of the gimbal system is defined in Fig. 3. The yaw axis rotating around Z_0 with θ_1 angle, the roll axis rotating around X_1 with θ_2 and the pitch axis rotating around Y_2 with θ_3 are represented by (X_0, Y_0, Z_0), (X_1, Y_1, Z_1) and (X_2, Y_2, Z_2), respectively.

The transformation matrices are derived in terms of rotation angles θ_1, θ_2 and θ_3 by using Denavit-Hartenberg (D-H) convention as

$${}^0_1T = \begin{bmatrix} c\theta_1 & -s\theta_1 & 0 & 0\\ s\theta_1 & c\theta_1 & 0 & 0\\ 0 & 0 & 1 & 0\\ 0 & 0 & 0 & 1\end{bmatrix},\quad {}^1_2T = \begin{bmatrix} 1 & 0 & 0 & 0\\ 0 & c\theta_2 & -s\theta_2 & 0\\ 0 & s\theta_2 & c\theta_2 & 0\\ 0 & 0 & 0 & 1\end{bmatrix},\quad {}^2_3T = \begin{bmatrix} c\theta_3 & 0 & s\theta_3 & 0\\ 0 & 1 & 0 & 0\\ -s\theta_3 & 0 & c\theta_3 & 0\\ 0 & 0 & 0 & 1\end{bmatrix} \tag{8}$$

$${}^0_3T = {}^0_1T^1_2T^2_3T \tag{9}$$

$${}^0_3T = \begin{bmatrix} c\theta_1c\theta_3 - s\theta_1s\theta_2s\theta_3 & -c\theta_2s\theta_1 & c\theta_1s\theta_3 + c\theta_3s\theta_1s\theta_2 & 0\\ c\theta_3s\theta_1 + c\theta_1s\theta_2s\theta_3 & c\theta_1c\theta_2 & s\theta_1s\theta_3 - c\theta_1c\theta_3s\theta_2 & 0\\ -c\theta_2s\theta_3 & s\theta_2 & c\theta_2c\theta_3 & 0\\ 0 & 0 & 0 & 1\end{bmatrix} \tag{10}$$

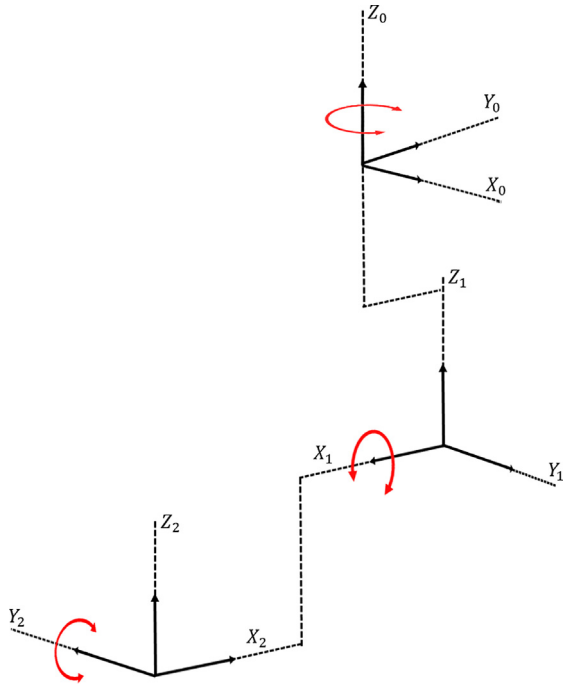

Fig. 3. Coordinate systems of three-axis gimbal system.

where $s\theta_i = sin(\theta_i)$ and $c\theta_i = cos(\theta_i)$ for $i = 1, 2, 3$. Here, ${}^{0}_{1}T$ is the transformation matrix of yaw axis from the frame of body 0 to the frame of body 1. Similarly, ${}^{1}_{2}T$ and ${}^{2}_{3}T$ are transformation matrices of roll and pitch axis from the frame of body 1 to body 2 and body 2 to body 3, respectively. The homogenous transformation from the base of gimbal system to the camera sensor coordinate frame is defined by the matrix ${}^{0}_{3}T$.

The aim of the mathematical model of three-axis gimbal system mounted on UAV is to find the target pose relative to the camera frame. In order to obtain the target pose in the camera frame, the position of the camera center at each instance is required. In this study, the IMU sensor is mounted on the camera frame, i.e. body 3 and position encoders mounted on servo motors. The angular position of the camera frame is derived from the gyroscopes and the accelerometers on the IMU mounted on it. The state of the camera relative to the target can be determined by making observations of the camera's position relative to the target. The camera position and orientation relative to the inertial frame are obtained from the sensor inputs.

Definition 3. A homogeneous transformation matrix that is used to define a rigid motion is derivated as

$$ {}^{i}_{g}T = \begin{bmatrix} {}^{i}_{c}R & {}^{c}_{i}P \\ 0 & 1 \end{bmatrix} = {}^{i}_{b}T\,{}^{b}_{g}T \tag{11} $$

$$ {}^{i}_{c}P = \left[{}^{i}_{c}T\right]^{-1} \tag{12} $$

where the transformation from inertial to camera frame is donated as ${}^{i}_{c}T$ which consists of a set of transformation from inertial to body frame ${}^{i}_{b}T$, from body fixed to gimbal frame ${}^{b}_{g}T$. The homogeneous transformation consists of a orthogonal rotation matrix ${}^{i}_{c}R$ that represents the orientation of the camera frame relative to the inertial frame. The column vector ${}^{c}_{i}P \in \Re^3$ denotes translation from the origin of the inertial frame to the origin of the camera frame. The angular position of the camera frame is derived from the gyroscopes and accelerometers on IMU mounted on gimbal system.

Definition 4. The errors of yaw, roll and pitch axes of camera's reference frame are defined as

$$ \mathcal{E}_i = \alpha_{d_i} - \alpha_i, i = 1, 2, 3 \tag{13} $$

where α_1, α_2 and α_3 are the angles of yaw, roll and pitch axes of camera frame on gimbal system, respectively. Also, α_{d_i} represents the desired position of the camera frame with respect to base frame of gimbal system mounted on UAV. The transformation matrix of camera's error reference frame is

$$ {}^{3}_{\varepsilon}T = \begin{bmatrix} c\varepsilon_1 c\varepsilon_3 - s\varepsilon_1 s\varepsilon_2 s\varepsilon_3 & -c\varepsilon_2 s\varepsilon_1 & c\varepsilon_1 s\varepsilon_3 + c\varepsilon_3 s\varepsilon_1 s\varepsilon_2 & 0 \\ c\varepsilon_3 s\varepsilon_1 + c\varepsilon_1 s\varepsilon_2 s\varepsilon_3 & c\varepsilon_1 c\varepsilon_2 & s\varepsilon_1 s\varepsilon_3 - c\varepsilon_1 c\varepsilon_3 s\varepsilon_2 & 0 \\ -c\varepsilon_2 s\varepsilon_3 & s\varepsilon_2 & c\varepsilon_2 c\varepsilon_3 & 0 \\ 0 & 0 & 0 & 1 \end{bmatrix} \tag{14} $$

where $s\varepsilon_i = sin(\mathcal{E}_i)$ and $c\varepsilon_i = cos(\mathcal{E}_i)$ for $i = 1, 2, 3$.

The joint angles of the three-axis gimbal system used in this study and shown in Fig. 1 are derived from the inverse kinematic analysis of the gimbal. The transformation matrix from base frame to the error frame $\mathcal{E}$ in camera's reference frame is

$$ {}^{0}_{\varepsilon}T(\theta, \mathcal{E}) = {}^{0}_{3}T(\theta)\,{}^{3}_{\varepsilon}T(\mathcal{E}) = \begin{bmatrix} t_{11} & t_{12} & t_{13} & 0 \\ t_{21} & t_{22} & t_{23} & 0 \\ t_{31} & t_{32} & t_{33} & 0 \\ 0 & 0 & 0 & 1 \end{bmatrix} \tag{15} $$

where θ which consists of θ_1, θ_2, and θ_3 is the current joint angle of the gimbal system, $\mathcal{E}$ which consist of $\mathcal{E}_1$, $\mathcal{E}_2$, and $\mathcal{E}_3$ is error vector, and t_{ij} represents the component of ${}^{0}_{3}T(\theta, \varepsilon)$. The new joint angle of the three-axis gimbal system is determined using Eq. (15) as

$$ {}^{0}_{3}T(\theta_{new}) = {}^{0}_{\varepsilon}T(\theta, \mathcal{E}) = {}^{0}_{3}T(\theta)\,{}^{3}_{\varepsilon}T(\mathcal{E}) \tag{16} $$

where ${}^{0}_{3}T(\theta_{new})$ indicates that frame of body 3 is same as error frame of camera frame. The desired joint angles of the three-axis gimbal system shown in Fig. 1 are derived as

$$ \theta_{new} = \begin{bmatrix} \theta_{1new} \\ \theta_{2new} \\ \theta_{3new} \end{bmatrix} = \begin{bmatrix} tan^{-1}\left(\frac{-t_{12}}{t_{22}}\right) \\ sin^{-1}(t_{32}) \\ tan^{-1}\left(\frac{-t_{31}}{t_{33}}\right) \end{bmatrix} \tag{17} $$

by the help of inverse kinematic analysis of the gimbal system.

In order to complete mathematical model of gimbal system actuator dynamics has been defined for brushless direct current (BLDC) servomotor. In the study, BLDC motor is used as the actuator in each joint of the three-axis gimbal system mounted on the UAV. The simplified mathematical model of the DC motor are shown in Fig. 4. The transfer function of each gimbal actuators to obtain desired position using controller for angular position θ_m and armature voltage V_a is given as

$$ \frac{\theta_m(s)}{V_a(s)} = \frac{K_m}{s[(L_a s + R_a)(J_m s + B_m) + K_m K_b]} \tag{18} $$

where K_m and K_b are moment and electromotive force constants, respectively. J_m, B_m, L_a, R_a are the moment of inertia of rotor, the damping ratio of mechanical system, armature resistance and armature inductance, respectively. Also, motor torque τ_m can be calculated

$$ \tau_m(s) = K_t I_a(s) = (J_m s + B_m) s\theta_m(s) \tag{19} $$

where I_a is the armature current and K_t is a physical constant.

The model of the three-axis gimbal system mounted on the UAV is simulated in the MATLAB environment. Note that the gimbal model is derived here in continuous time. One can easily sample input-output values using appropriate sampling frequency. The change of each element of the mass matrix of the three-axis gimbal system mounted on UAV according to time can be examined with the help of this model. Even though the nonlinear gimbal system dynamic can be simulated for given

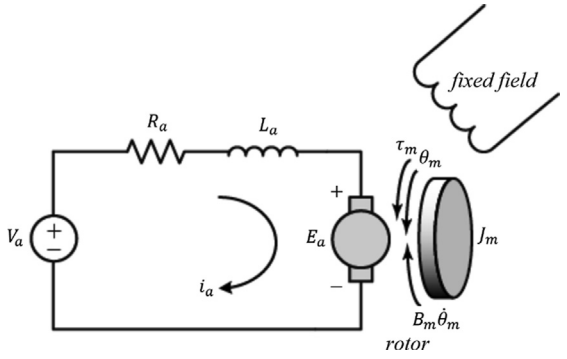

Fig. 4. Mathematical model of DC motor.

actuator input voltage and angular output position, model based controller design procedure needs simplified input-output models. Following section we propose linear and nonlinear model structures for given input-output data.

4. System identification for gimbal system on UAV

System identification is the process of obtaining mathematical model from a dynamic system based on input-output data. In cases where system gain and dynamic behavior of the system need to be determined, modeling becomes important. Obtaining an appropriate mathematical model of the system enables the analysis of the dynamic system. The dynamic system model for a physical system includes mathematical model with input-output parameters [29]. The purpose of the system identification is to "create a model with adjustable parameters and then set these parameters to match the predicted output to match the measured output" [30]. With the system identification, it is aimed to determine an unknown transfer function for linear systems and to obtain a mathematical model which gives input-output relationship for non-linear systems. In order to create a dynamic system model by using experimentally collected data, data processing, model structure and appropriate model determination steps are carried out [29]. The three-axis gimbal system identification steps consist of data collection, data processing, model structure selection, parameter estimation and model verification steps as shown in Fig. 5. All of these stages are of great importance for the correct determination of system dynamic behavior. The input-output data for the three-axis gimbal system to be modeled is obtained with the help of special experimental devices designed for system identification. The most difficult and most important phase of the system identification process is to determine the most appropriate model structure for the system. Whether the model is to be constructed in a linear or nonlinear structure is determined by mathematically pre-calculating the input-output parameters and disturbing effect parameter values related to the model. The general input-output linear model is defined as

$$A(q)y(k) = \frac{B(q)}{F(q)}u(k) + \frac{C(q)}{D(q)}e(k) \tag{20}$$

where input input u, output y, and external disturbance e at time k. In Eq. (20), q is the delay operator and A, B, C, D, and F polynomials for defined order. For linear dynamic systems as in Eq. (14), auto regressive with exogenous input (ARX) where F, C, and D polynomials are unity, auto regressive moving average with exogenous input (ARMAX) where F and D polynomi-

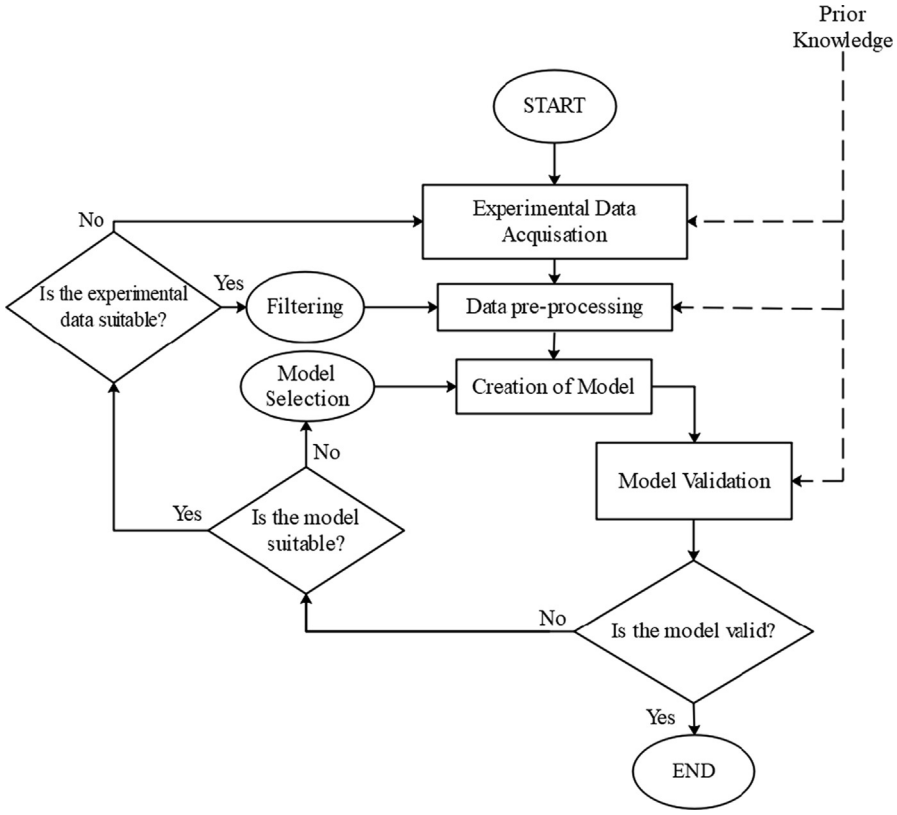

Fig. 5. The three-axis gimbal system identification flow chart.

als are unity, auto regressive moving average (ARMA) where B, F, and D polynomials are unity, Box-Jenkins (BJ) where A polynomial is unity and OE where A, C, and D polynomials are unity are commonly used parametric model structures [29–31].

In addition, not only dynamic linear but also static nonlinear block oriented model structures, i.e., Wiener and Hammerstein are shown in Fig. 6, Wiener-Hammerstein, Hammerstein-Wiener, are used frequently in the identification of nonlinear systems, but also general input-output Volterra/Wiener, nonlinear autoregressive exogenous (NARX), nonlinear autoregressive and moving average (NARMA) and external input NARMA model structures are used [29,31–33]. In this study, OE model which is least affected by external disturbances according to other linear system identification models and Hammerstein model which has static nonlinear and dynamic linear blocks are used both to deal with nonlinearity and to robust control of the gimbal system under external disturbances.

4.1. OE model

The main difference between model structures is due to the effects of external disturbances on modeling. The OE model shown in Fig. 7 is defined by

$$y(k) = \frac{B(q)}{F(q)}u(k) + e(k) \tag{21}$$

where system dynamics can be defined separately and have the advantage of not wasting any parameters in a disturbing model [30]. In Eq. (21), the external disturbance $e(k)$, Gaussian white noise (GWN) [29], applied to the system is expressed with system input $u(k)$ and system output $y(k)$. The polynomial $B(q)$ and $F(q)$ are stated as

$$B(q) = b_0 + b_1 q^{-1} + b_2 q^{-2} + \cdots + b_{k-1} q^{-(k-1)} \tag{22}$$

$$F(q) = 1 + f_1 q^{-1} + f_2 q^{-2} + \cdots + f_k q^{-k} \tag{23}$$

The parameters of the OE model structure are estimated here using prediction error method (PEM).

The output signal $y(k)$ of the system is defined as

$$y(k) = -f_1 \hat{y}(k-1) - f_2 \hat{y}(k-2) - \cdots - f_N \hat{y}(k-N) + b_0 u(k) + b_1 u(k-1) + \cdots + b_M u(k-M) + e(k) \tag{24}$$

where the output signal of the system depends on the current and previous input signals, the previous output signals and $f_i, b_j (i = 1, \cdots, N, j = 0, \cdots, M)$ the transfer function coefficients. Also, the Eq. (24) is described in vector form as

$$y(k) = \hat{\varphi}^T(k)\theta + e(k) \tag{25}$$

where regresor vector $\hat{\varphi}^T$ and parameter vector θ are defined as

$$\hat{\varphi}(k) = \left[-\hat{y}(k-1) \quad -\hat{y}(k-2) \cdots -\hat{y}(k-N) \quad u(k) \quad u(k-1) \cdots u(k-M) \right]^T$$

$$\theta = \left[f_1 \quad f_2 \cdots f_N \quad b_0 \quad b_1 \cdots b_M \right]^T$$

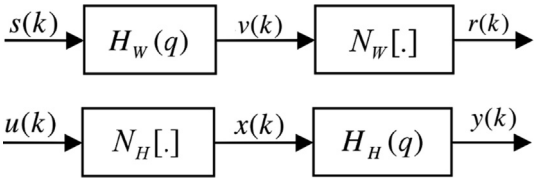

Fig. 6. Wiener and Hammerstein model block structure.

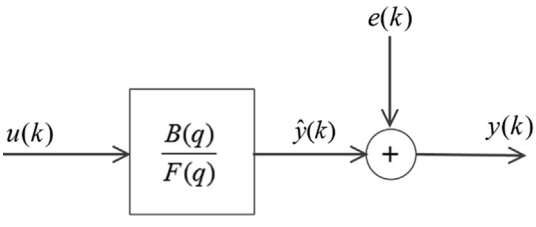

Fig. 7. OE model block structure.

In Eq. (25), the regressor vector and the parameter vector are represented by $\widehat{\varphi}(k)$ and θ, respectively. The regressor vector $\widehat{\varphi}(k)$ depends on the past estimated output values and the current and past input values. All elements of the regressor vector are input–output data measured on the system. The estimated $\widehat{\theta}$ vector is expressed as

$$\widehat{\theta} = \left[\sum_{k=0}^{K-1} \widehat{\varphi}^T(k)\widehat{\varphi}(k)\right]^{-1}\left[\sum_{k=0}^{K-1} \widehat{\varphi}(k)y(k)\right] \qquad k = 0, 1, \cdots K-1 \tag{26}$$

when there is disturbing signal white noise affecting the system,

$$G(q^{-1}, \theta) = \frac{B(q^{-1})}{F(q^{-1})} \tag{27}$$

and the estimated output signal is obtained as

$$\widehat{y}(k|\theta) = B(q^{-1})u(k) + \left[1 - F(q^{-1})\right]y(k) \tag{28}$$

In this study, the OE model, which enables us to obtain the nearest parameter estimation as to its actual value [30], is used for the linear identification of the three-axis gimbal system and its performance is compared with the nonlinear system identification model as well as to show system nonlinearity.

4.2. Hammerstein model

The physically realized engineering systems are usually designed in a nonlinear structure. When the mathematical model of the gimbal system mounted on the UAV is examined, it is seen that the gimbal system works in the nonlinear region due to saturation. It is not always possible to obtain mathematical equations and analytical solutions of nonlinear systems such as the gimbal system mounted on the UAV. Therefore, nonlinear systems are linearized under certain conditions and constraints. The conformity of the linearized system to the real system determines the performance of the model [29]. The Hammerstein block structure comes to the fore in obtaining the model of the system to be controlled to ensure the model-based control of the nonlinear gimbal system [34]. The Hammerstein model structure consists of a static nonlinear block followed by a linear dynamic subsystem as shown in Fig. 6. $N_H[.]$ shown in Fig. 6 is a static nonlinear function such as polynomial, piecewise, monotone nonlinearity. The purpose of the identification is to estimate the coefficients $\{a_i, b_i\}$ of the polynomials $A(q)$, $B(q)$ and the parameters of the nonlinear $N_H[.]$ function by means of the current input–output $\{u(k), y(k)\}$ data [35]. When the input signal $u(k)$ is applied to the system shown in Fig. 8, the input signal first interacts with the nonlinear Hammerstein block of the system and the obtained $x(k)$ signal is the input signal of the linear block of the system. The output of the linear block of the system is obtained as system output $y(k)$. In the system identification part of this study, GWN which any two values are statistically independent, regardless of how close they are in time is used as an external disturbance $e(k)$.

The linear and nonlinear blocks of the system shown in Fig. 8 are mathematically expressed as

$$x(k) = \alpha_1 u(k) + \alpha_2 u^2(k) + \cdots + \alpha_R u^R(k) \tag{29}$$

$$y(k) = -a_1\widehat{y}(k-1) - a_2\widehat{y}(k-2) - \cdots - a_N\widehat{y}(k-N) + b_0 x(k) + b_1 x(k-1) + \cdots + b_M x(k-M) + e(k) \tag{30}$$

Also, Eq. (30) can be written in vector form as

$$\hat{y}(k) = \left[-\hat{y}(k-1)\cdots-\hat{y}(k-N)\,u(k) \quad u(k-1)\cdots u(k-M)\cdots u^R(k)\cdots u^R(k-M)\right]\begin{bmatrix} a_1 \\ \cdots \\ a_N \\ b_0\alpha_1 \\ \cdots \\ b_0\alpha_R \\ b_1\alpha_1 \\ b_1\alpha_2 \\ \cdots \\ \vdots \\ b_M\alpha_R \end{bmatrix} \tag{31}$$

$$\widehat{y}(k) = \widehat{\varphi}^T(k)\theta \tag{32}$$

where the parameter vector θ and the regressor vector $\widehat{\varphi}^T(k)$ depends on the past output values and the current and past input values.

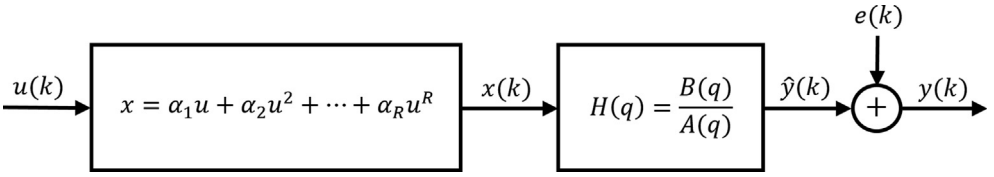

Fig. 8. Hammerstein model linear and nonlinear block structure.

In Eq. (31), the coefficients a_i, b_j and α_m $(i = 1, \cdots, N, j = 0, \cdots, M, m = 1, \cdots, R)$ in the parameter vector θ are determined by means of the input signal $u(k)$ and the output signal $y(k)$. One can separate a_i and b_j coefficients in Eq. (31) by using least aquares approach as in [32,34]. All elements of the regressor vector are input–output data measured on the system with the data length of K. The estimated $\widehat{\theta}$ vector is expressed as

$$\widehat{\theta} = \left[\sum_{k=0}^{K-1} \widehat{\varphi}^T(k)\widehat{\varphi}(k)\right]^{-1}\left[\sum_{k=0}^{K-1} \widehat{\varphi}(k)y(k)\right] \qquad k = 0, 1, \cdots K-1 \tag{33}$$

The accuracy of the modeling of three-axis gimbal system mounted on UAV depends on the fact that the error of estimation is Gaussian distribution and independent of the input signal. The autocorrelation function, which is defined as,

$$\widehat{R}_\varepsilon(\tau) = \frac{1}{K}\sum_{k=0}^{K-1} \varepsilon(k)\varepsilon(k-\tau) \tag{34}$$

is examined to test whether the error of estimation is Gaussian distribution. The cross-correlation function defined as,

$$\widehat{R}_{\varepsilon u}(\tau) = \frac{1}{K}\sum_{k=0}^{K-1} \varepsilon(k)u(k-\tau) \tag{35}$$

is examined to determine whether the estimation error is related to the input signal. Also, in the study, maximum likelihood-expectation maximization (ML-EM) approach [36] is used to estimate the parameter vector θ based on input and output measurements of the three-axis gimbal system. ML-EM has guaranteed parameter convergence of stable estimated system not only for Gaussian but also other distribution while disturbance and the system input are independent [37].

5. MPC controller design for three-axis gimbal system mounted on UAV

The MPC is characterized a controller class that calculates the control sequence that must be implemented to optimize the future behavior of the system. The inadequacy of conventional control methods in cases such as remove the dead-time in plant, time delays in multivariable systems, open-loop unstability and overcome the constraints has played an important role in the development of MPCs [38]. The system model, the disturbance model and the MPC algorithms differ according to the criteria to be minimized [39,40].

The MPC algorithm optimizes the behavior of the system in the future in each control interval. The MPC calculates the inputs and outputs of the process in the future using the system model and the instantaneous measurements taken from the system. This calculation is carried out as a solution to an optimization problem which is formed according to the desired criteria.

Definition 5. Given the cost function

$$J\Big(y(k), \Delta u(k), N_p, N_c\Big) = \sum_{j=N_1}^{N_p} w_j[y(k+j|k) - r(k+j)]^2 + \sum_{j=N_1}^{N_c} \lambda_j\Big[\Delta u(k+j-1|k)\Big]^2 \tag{36}$$

MPC optimization for a dynamic system can be obtained mathematically in the form of

$$u(k) = \min_{u(k|k),\cdots u(k+N_c-1|k)} J(N_1, N_p, N_c) \tag{37}$$

subject to

$$u_{min} \le u(k+j-1|k) \le u_{max} \qquad j = N_1, \cdots, N_c \tag{38}$$

$$-\Delta u_{max} \le \Delta u(k+j-1|k) \le \Delta u_{max} \tag{39}$$

$$y_{min} \le y(k+j|k) \le y_{max} \qquad j = N_1, \cdots, N_p \tag{40}$$

where $y(k+j|k)$ is an optimum j step ahead prediction of the system output on data up to sample k, N_1, N_p and N_c are min/-max prediction and control horizon, w_j and λ_j are weighting sequences, respectively. $u(k+j-1|k)$ is an sequence of input signals to be sent from the controller to the plant in the future. Also, u_{min} and u_{max} are the boundary conditions of the system input, y_{min} and y_{max} are the boundary conditions of the system output and Δu is the difference between the current input signal and the previous input signal $(\Delta u(k) = u(k) - u(k-1))$. Note that $y(k+j|k)$, j step ahead prediction of system output is calculated using Eqs. (29) and (30) for Hammerstein model where the input is $u(k+j-1|k)$.

The objective of predictive control is to compute the future control sequence $u(k)$, $u(k+1), \cdots, u(k+N_c)$in such a way that the future plant output $y(k+j)$ is driven close to future reference trajectory $r(k+j)$. The reference value as input, the measured disturbance signal and system output signal are applied to the MPC block and future inputs-outputs of the system are determined by optimizing the with the help of the Eq. (37).

MPC algorithms differ from each other in terms of the model used and the performance criteria selected. The dynamic matrix control, model algorithmic control and generalized predictive control algorithms are frequently used among MPC algorithms. Appropriate cost functions are determined with each MPC algorithm to determine the controlling rule. The general purpose in the cost function is to follow a predetermined reference signal of the future system output in the desired prediction horizon and to penalize by holding the required control signal within certain limits [38]. The coefficients w_j and λ_j are sequences that consider the future behaviour. These coefficients are usually selected as constant values or exponential sequences. The step response model from the commonly used models in MPC algorithms is used in dynamic matrix control algorithms and multivariate systems. The reason for the widespread use of this model is that the system output can be measured by applying step input to the system and the model parameters can be easily determined. We get such a model using Eqs. (29) and (30) for nonlinear Hammerstein based MPC as well as using Eq. (24) for OE. Due to nonlinearity of three-axis gimbal system we used Hammerstein model instead of OE to MPC based control of gimbal system mounted on UAV where processes described in [41] have been applied in the design of MPC controller.

6. Simulation and experimental study

6.1. Experimental setup

In the study, the input-output data of gimbal mounted on the UAV which has joints and mechanical structure shown in Fig. 9 are obtained experimentally under external disturbance. The experimental data of the gimbal mounted on the UAV is taken in the environment which has a wind speed of 5.6 m/sec in the South-East (SE) direction. In order to identify models of the gimbal under the external disturbance, in addition to the wind in the environment, the disruptive force is applied to the yaw-pitch and pitch-roll axes by means of external servo motor experiment setup. The data sets consisting of the experimental data are divided into two parts for system identification and model validation. The model of the system is created with the help of the system identification data in the first part and the validity of the system model created by the model verification data in the second part is tested. In the determination of three-axis gimbal system model degrees mounted on UAV, the data set allocated for system identification is used. The degree of system models obtained is determined according to the Akaike Information Criteria (AIC) and Final Prediction Error (FPE) [29]. The validity of the gimbal models obtained by cross correlation and auto correlation is determined.

The gimbal system mounted on the UAV shown in Fig. 9 is operated for 425 s and 8500 data is obtained with the sampling time $T = 0.05$ s. In order to create the model of the three-axis gimbal system mounted on the UAV under external disturbance, external disturbance in the form of two times pulse is applied to firstly the pitch axis and then roll axis of the gimbal system in 175th second of experimental study by aid of a servo motor with a speed of 70 rpm at 6 V and a torque of 0.484

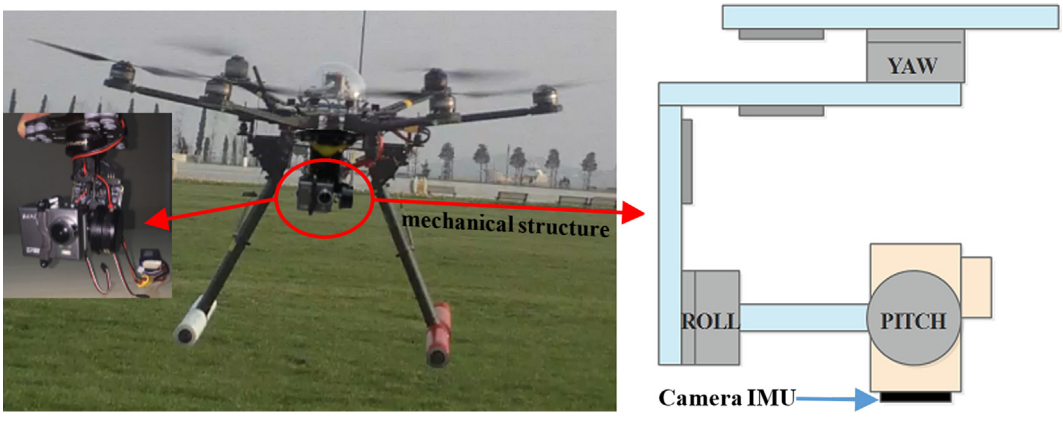

Fig. 9. Three-axis gimbal system and mechanical structure mounted on UAV.

Nm. The disruptive pulse has been applied to the pitch and roll axes at a 45° angle so that the three-axis gimbal system is exposed to the maximum level of external disturbance. The linkage lengths of the three-axis gimbal system used in the study are 30 *mm*, 35 *mm* and 25 *mm* respectively for the first, second and third joints, and their weights are 25 g, 155 g and 30 g respectively for the first, second and third joints. There is a 150 g weight camera and 5 g weight camera mounting apparatus on the pitch axis of the gimbal system. The position of the camera located on the pitch axis of the gimbal system is set to 1° angle and the reference angle value is determined. The position values of the BLDC servomotors in the joints are obtained by means of the encoders on them.

6.2. Model identification and validation

In this study, the data set consisting of $K = 8500$ data obtained experimentally is used to obtain the model of the three-axis gimbal system with the sampling frequency of 20 *Hz*. The data set used is divided into two parts, the first part consisting of 3500 data and the second part consisting of 5000 data. The experimental data in the first part are taken in environment which has a wind speed of 5.6 m/sec in the SE direction as the external disturbance. The experimental data in the second part are taken under the disruptive pulse applied to the pitch and roll axes of the gimbal system with an angle of 45° in addition to the wind speed in the environment. The input–output dataset for the three-axis gimbal system mounted on UAV is shown in Fig. 10 where the input is torque and the output is position. The three-axis gimbal system model order according to the AIC and FPE criteria is determined three for OE as well as for Hammerstein system linear and nonlinear part.

The linear OE and nonlinear Hammerstein models which are shown in Figs. 11 and 12, respectively of three-axis gimbal system are obtained when there is no disturbance effect except wind speed in the environment by aid of the system identification data in the first part. For the case where there is no external disturbance effect except wind speed in the environment, the model parameters of thee-axis gimbal system are estimated by ML-EM and the gimbal system is modeled with OE and Hammerstein models with 92.81% and 97.26% performance, respectively.

One can observed that the model identification structure which has the least complexity, minimizes the estimation error, is obtained by Hammerstein model when the parametric model structures are analyzed and the OE and Hammerstein model estimation errors are examined for the identified three-axis gimbal system model and the three-axis gimbal system to be controlled. The nearest values to the coefficients defined for the input and output functions are obtained by the identified Hammerstein model structure and gimbal system model with the least complexity is defined by the Hammerstein model identification structure. When the values calculated as physical three-axis gimbal system output and Hammerstein model identification output are compared with each other, it is seen that the results are compatible.

The linear OE and nonlinear Hammerstein models which are shown in Figs. 13 and 14 respectively of three-axis gimbal system are obtained when the disruptive pulse applied to the pitch and roll axes of the gimbal system two times with an angle of 45° in addition to the wind speed in the environment by aid of the system identification data in the second part.

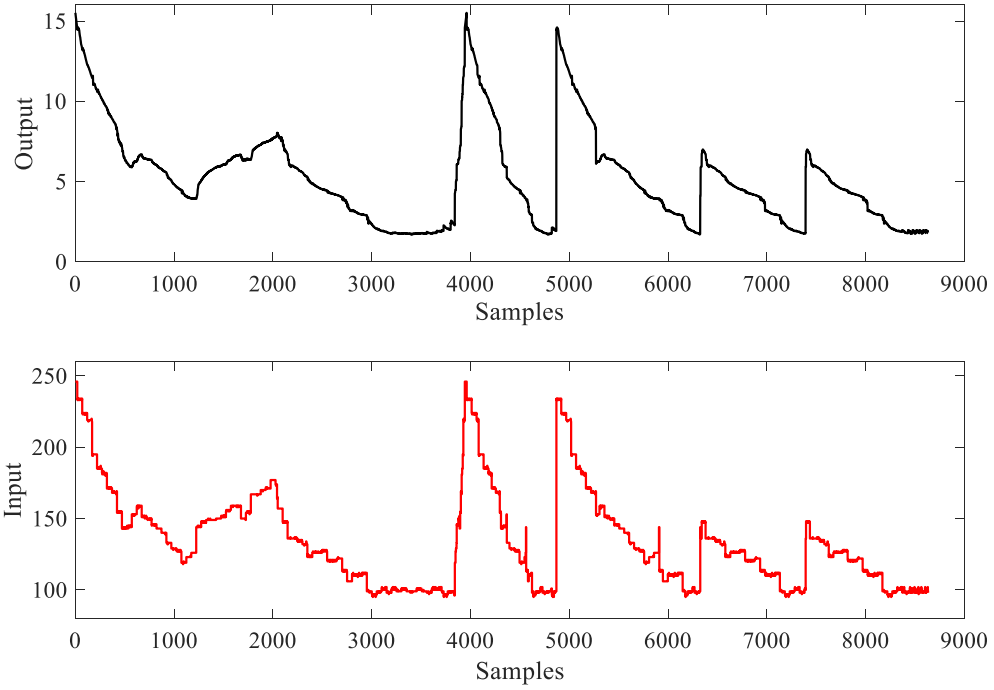

Fig. 10. Input-output data of three-axis gimbal system mounted on UAV.

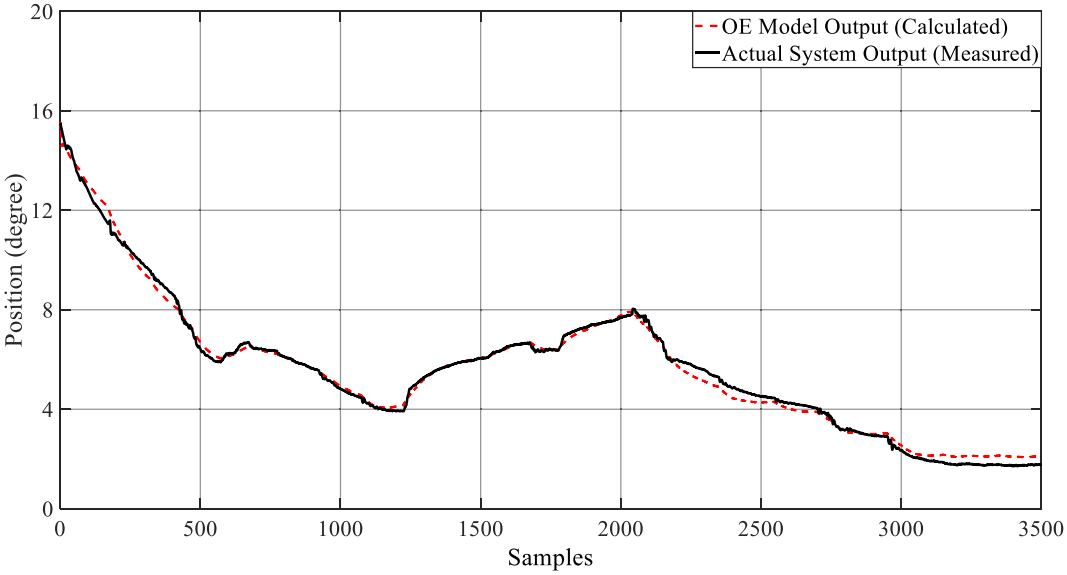

Fig. 11. OE model of the three-axis gimbal system with external disturbance wind effect.

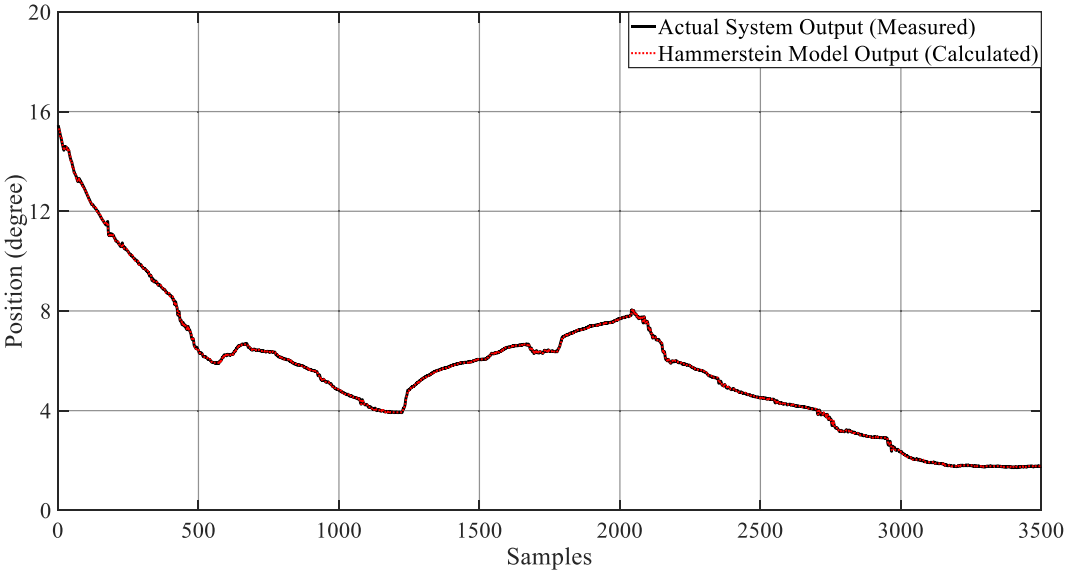

Fig. 12. Hammerstein model of the three-axis gimbal system with external disturbance wind effect.

When the external disturbance is applied, it is observed that the deviation in the pitch axis of the three-axis gimbal is maximum 14° according to the reference angle value of 1° and the deviation in the roll axis of the three-axis gimbal is maximum 6° according to the reference angle value of 1°.

The model parameters of thee-axis gimbal system are estimated by the least squares method and the gimbal system is modeled with OE and Hammerstein models with 89.17% and 96.48% performance respectively under the external disturbance in addition to the wind speed in the environment. The linear OE and nonlinear Hammerstein models which are shown in Fig. 15 and Fig. 16 respectively of the three-axis gimbal system are obtained using all the data sets which are presented in Fig. 10 collected experimentally. When the system model obtained which is obtained when no external disturbance except wind speed in the environment is applied to the three-axis gimbal system mounted on UAV defined by using all data sets, the performance is determined as 91.46% for OE model and 96.98% for Hammerstein model. According to the AIC and FPE criteria, the degree of the system model is determined as 3. Third-order transfer function for OE model of the three-axis gimbal system mounted on the UAV under external disturbance is obtained as

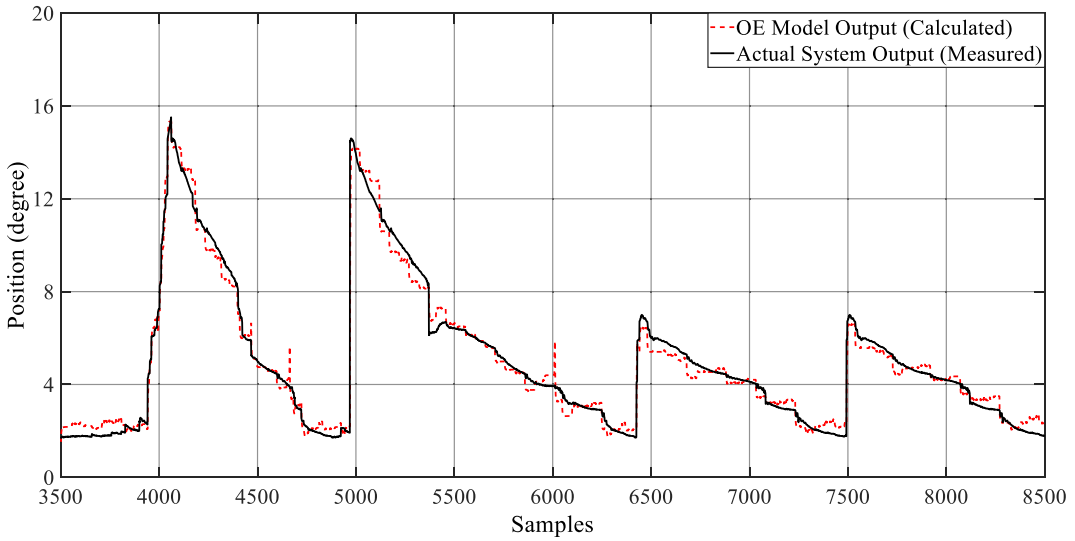

Fig. 13. OE model of the three-axis gimbal system under external disturbance with disruptive pulses.

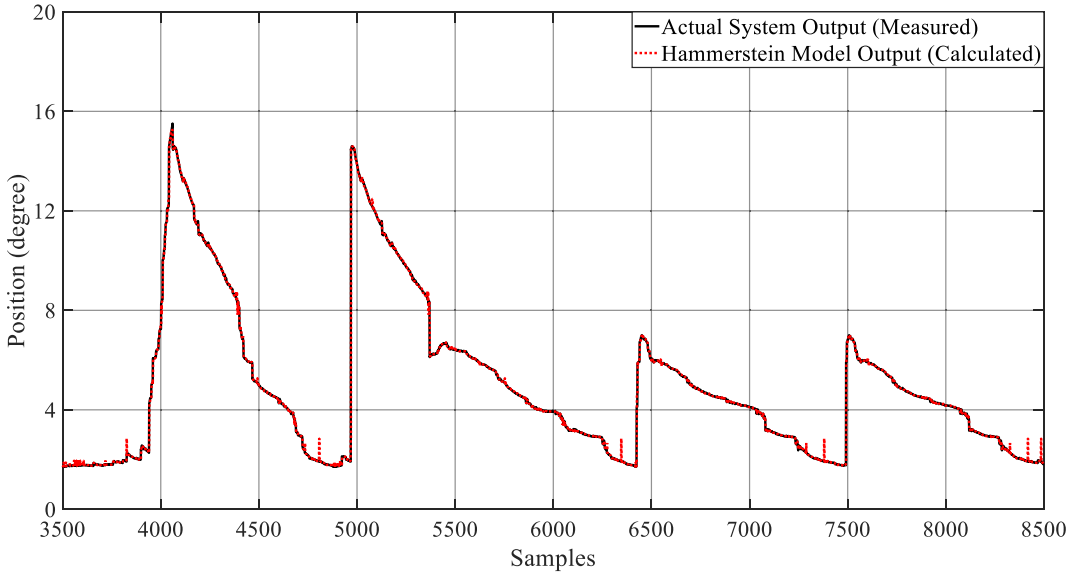

Fig. 14. Hammerstein model of the three-axis gimbal system under external disturbance with disruptive pulses.

$$\widehat{y}(k) = \frac{0.0565q^{-1} - 0.565q^{-2}}{1 - 1.131q^{-1} - 0.1015q^{-2} + 0.2325q^{-3}}u(k) \tag{41}$$

The linear and nonlinear blocks of the Hammerstein model of the three-axis gimbal system mounted on the UAV under external disturbance is obtained in the form of

$$x(k) = 2.7582u(k) - 1.8672u^2(k) + 3.1377u^3(k) \tag{42}$$

$$\widehat{y}(k) = \frac{0.0305q^{-1} - 0.4308q^{-2}}{1 - 1.3313q^{-1} - 0.6671q^{-2} + 0.7203q^{-3}}x(k) \tag{43}$$

The behavior of the three-axis gimbal system is defined by the input–output data and is embedded offline to the control card mounted on the UAV for real-time application. Thanks to the model of the identified third order gimbal system, the implementation complexity of the proposed MPC controller is minimized. Instead of OE we use Hammerstein for MPC due to nonlinearity that is shown clearly in this identification process.

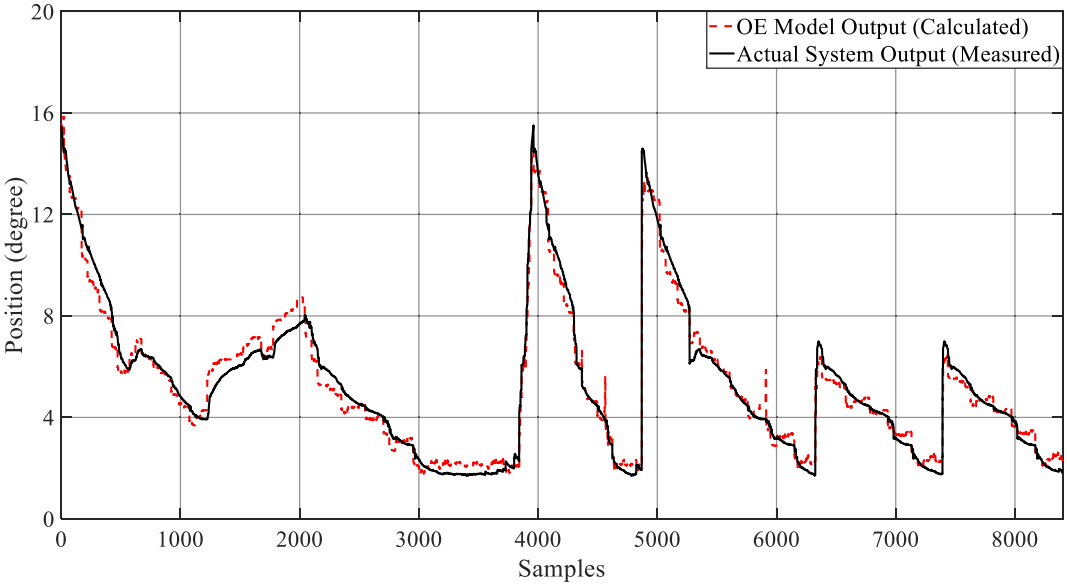

Fig. 15. OE model of the three-axis gimbal system mounted on UAV.

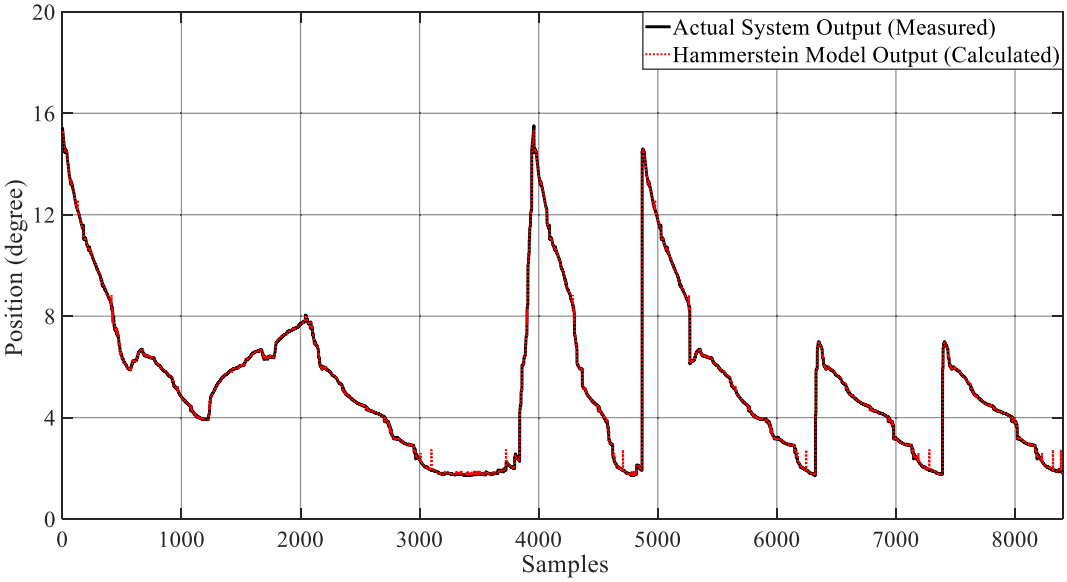

Fig. 16. Hammerstein model of the three-axis gimbal system mounted on UAV.

The residual autocorrelation and cross correlation function of the obtained Hammerstein model is shown in Fig. 17. When the system is modeled with high performance, it is expected that the function will produce values close to zero.

It is seen that the autocorrelation and cross correlation graphs shown in Fig. 17 are within the determined band spacing, and the autocorrelation coefficients of the errors are found to be within the 95% confidence level and $\pm 1.96/\sqrt{K}$ limit values.

6.3. Performance comparison of MPC and PID controllers

The control of the three-axis gimbal system mounted on UAV shown in Fig. 9 is performed with both the conventional PID controller and the MPC controller which is designed based on the Hammerstein model. In the implementation of the MPC method, it is important to either improve the optimization method or improve the computation speed in respective from hardware implementation [42–44]. The control scheme of the proposed model-based controller for the three-axis gimbal system is depicted in Fig. 18. The inputs of the Hammerstein model are past control actions, output signal and future control

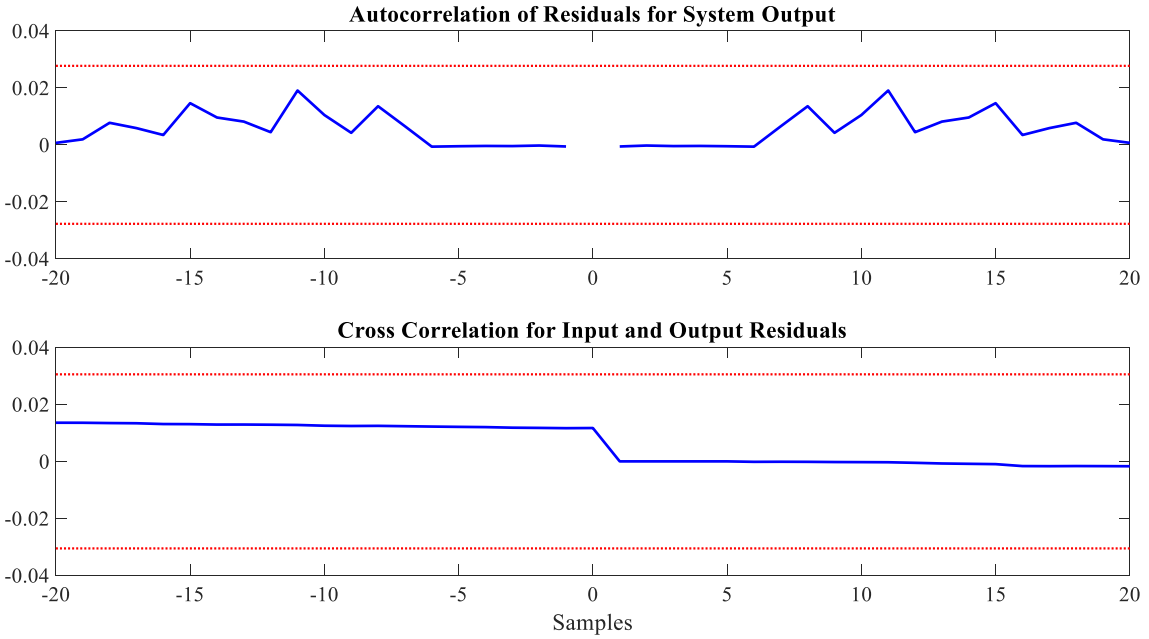

Fig. 17. Autocorrelation and cross correlation of three-axis gimbal system mounted on UAV.

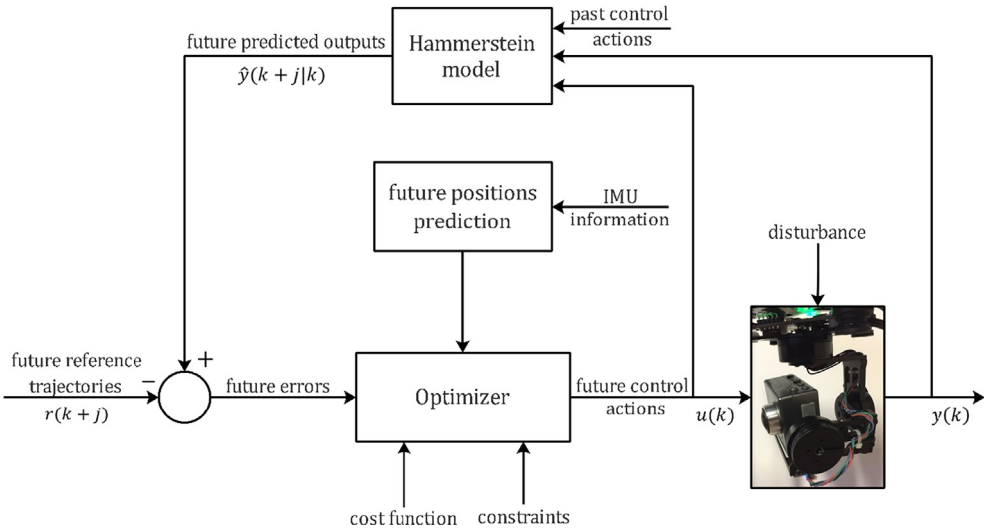

Fig. 18. MPC based control scheme of the proposed controller for target tracking.

actions. The future errors between future predicted outputs and future reference trajectories is optimized and the future control actions in the output of the optimizer are sent to both the model and the system as input. The performance of both proposed controller and PID controller has been tested for real-time target tracking under external disturbances by using three different geometry paths such as rectangular, circular and lemniscate (∞). In this study, the Hammerstein model obtained for target tracking is embedded in the TMS320F28335 eZdsp digital signal processing (DSP) prototyping card shown in Fig. 19 on the UAV which has three-axis gimbal system shown in Fig. 9. The TMS320F28335 eZdsp DSP prototyping card consists of a 32-bit CPU and a single-precision 32-bit floating-point [45]. The 150 MHz system clock is provided by an on-chip oscillator. The application of TMS320F28335 DSP employed with digital fabricated board is shown in Fig. 20. It consists of PWM interfaces for AC drive system, I/O interfaces for DC drive system, digital to analog converter (DAC), analog to digital converters (ADC) and encoder for the rotor speed detection.

The performance in determining the gain parameters directly affects the performance of the PID controller. Therefore, in the study, the gain parameters of the PID controller are determined by the Ziegler-Nichols method. The gain parameters of

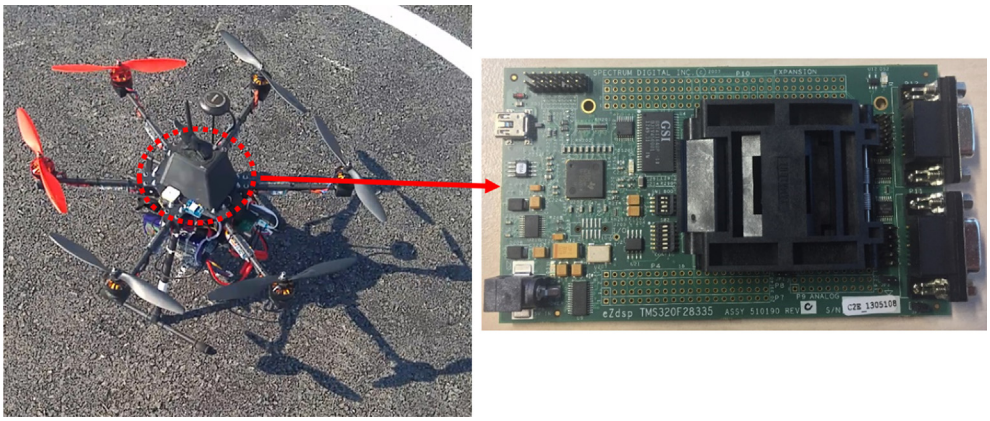

Fig. 19. DSP prototyping card on UAV used for real-time target tracking.

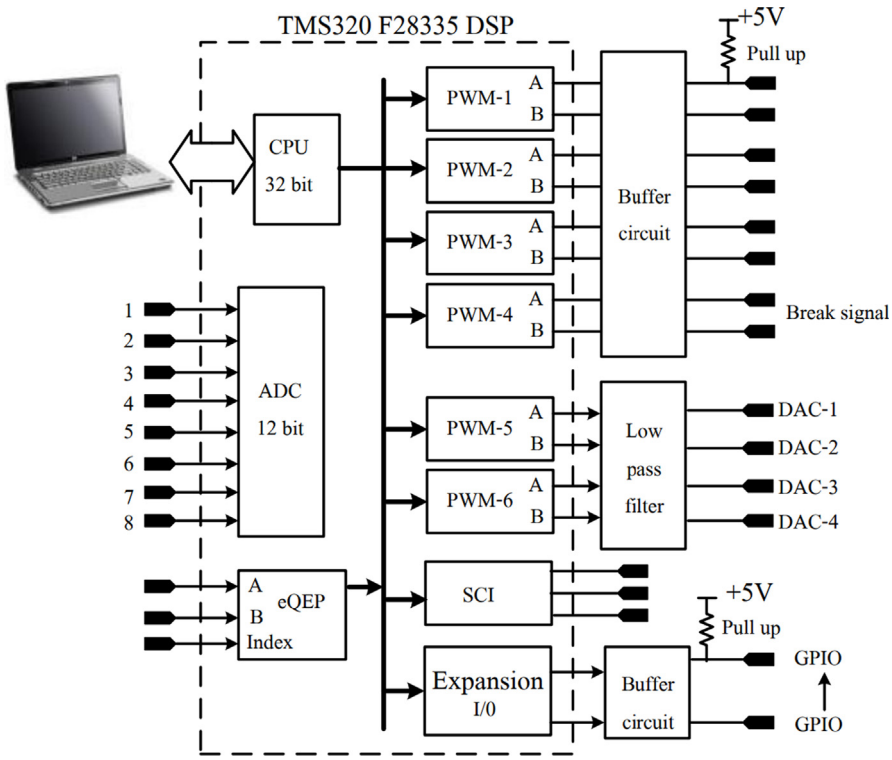

Fig. 20. The architecture of DSP card.

the traditional PID controller are determined using the Ziegler-Nichols method according to the system response analysis performed on the mathematical model of the three-axis gimbal system created in MATLAB. The design parameters of the gimbal system for target tracking are determined as maximum overshoot $M_P \leq \%2.5$, rise time $t_r \leq 0.35$ *sec*, settling time $t_s \leq 0.9$ *sec*, and steady state error $e_{ss} < 0.1$. The PID gain parameters are established as $K_P = 0.284$, $K_I = 0.059$ and $K_D = 0.139$. The MPC parameters are determined $N_1 = 3, N_p = 12$, and $N_c = 6$. The DSP card computational time of control input for each step is 0.01 sec for MPC using Hammerstein model, 0.02 sec for PID while sampling time is 0.05 sec. Even-though PID computational time is faster than MPC both control input signal can be calculated for each step. The convergence speed of the proposed MPC algorithm is determined by prediction horizon and control horizon values. In the control of the gimbal system, when the prediction horizon value is increased by keeping the control horizon value is constant, the overshoot and settling time values decrease. Also, when the control horizon value is increased by keeping the prediction horizon value by keeping the prediction horizon value is constant, the overshoot value of the system increases. In the MPC control of the three-axis gimbal system, Hammerstein model with higher model performance than the OE model is used.

The following three scenarios have been studied in order to evaluate the performance of the PID and MPC controllers in the three-axis gimbal system for real time target tracking under external disturbances. UAV, which has three-axis gimbal system, camera, GPS, telemetry and flight control card, such as equipment has carried out autonomously three different mission flights in outdoor enviorenment. All flight test scenarios are performed at the fixed altitude of 10 m for both of the control algorithms. During the flight test scenario in outdoor enviorenment is shown in Fig. 21. The mission flight has been repeated 10 times and averaged to get mission flight time as well as UAV battery levels have been measured at the end of the mission flight. The total error is calculated as summing up distance between reference path and gimbal system position for each sample.

In the first scenario, MPC and PID performance of the three-axis gimbal system are tested in real-time target tracking for the path in the form of rectangular geometry in environment which has an average wind speed of 6.2 m/sec in the SE direction as the external disturbance that is bounded as in Def. 2. The trajectory which has rectangular geometry is followed by PID and MPC controllers as shown in Fig. 22. The maximum error for PID and MPC controllers is determined as 4.85 m and 0.54 m, respectively. The total error for PID and MPC controllers is determined as 157.21 m and 12.39 m, respectively. The mission flight has been completed at 47 sec with the PID controller and at 35 sec with the MPC controller. The average speed of UAV with PID and MPC algorithms has been measured 3.08 m/sec and 4.14 m/sec, respectively. It has been observed that the UAV completes the mission flight with PID and MPC control algorithms by consuming approximately 29% and 18% energy, respectively.

In the second scenario, MPC and PID performance of the three-axis gimbal system are tested in real-time target tracking for the path in the form of circular geometry in environment which has a wind speed of 6.3 m/sec in the SE direction as shown in Fig. 23. The maximum error for PID and MPC controllers is determined as 4.27 m and 0.68 m, respectively. The total error for PID and MPC controllers is determined as 172.15 m and 10.26 m, respectively. The mission flight has been completed at 54 sec with the PID controller and at 43 sec with the MPC controller. The average speed of UAV with PID and MPC algorithms has been measured 2.03 m/sec and 2.55 m/sec, respectively. It has been observed that the UAV completes the mission flight with PID and MPC control algorithms by consuming approximately 24% and 15% energy, respectively.

In the third scenario, MPC and PID performance of the three-axis gimbal system are tested in real-time target tracking for the path in the form of lemniscate (∞) geometry in environment which has a wind speed of 6.1 m/sec in the SE direction as shown in Fig. 24. The maximum error for PID and MPC controllers is determined as 3.17 m and 0.38 m, respectively. The total error for PID and MPC controllers is determined as 105.82 m and 6.39 m, respectively. The mission flight has been completed at 51 sec with the PID controller and at 39 sec with the MPC controller. The average speed of UAV with PID and MPC algorithms has been measured 2.54 m/sec and 3.33 m/sec, respectively. It has been observed that the UAV completes the mission flight with PID and MPC control algorithms by consuming approximately 20% and 13% energy, respectively. The mean squared error (MSE) values for the three scenarios performed with PID and MPC controllers are presented in Table 1. When Figs. 22–24 obtained for three scenario are examined, it is seen that the performance of three-axis gimbal system mounted on UAV which has MPC controller based on Hammerstein model is very successful and robust compare to the UAV which has PID controller. Compare to PID, MPC based gimbal system control performance has been improved 92.11%, 94.04, 93.96%, for each scenarios in Table 1 respectively.

Performance comparison based on PID, it is guaranteed that the maximum and total error performance of the UAV in real-time target tracking under external disturbances is improved by at least 23% with the proposed Hammerstein based MPC comparing to the fuzzy PID controller [23] performance in following of trajectories with various geometries.

Fig. 21. Flight test scenario in outdoor environment.

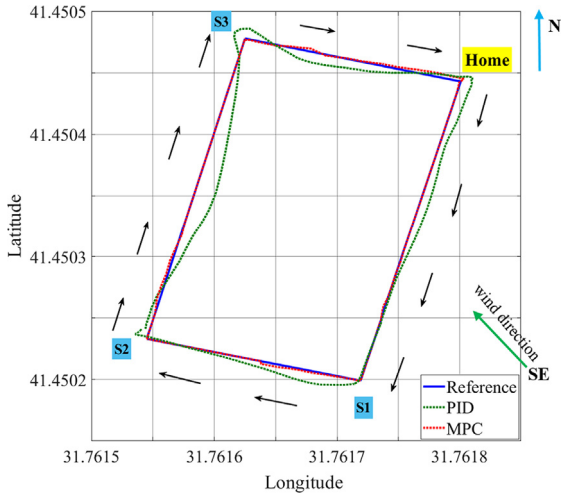

Fig. 22. MPC and PID performance of the three-axis gimbal for the first scenario.

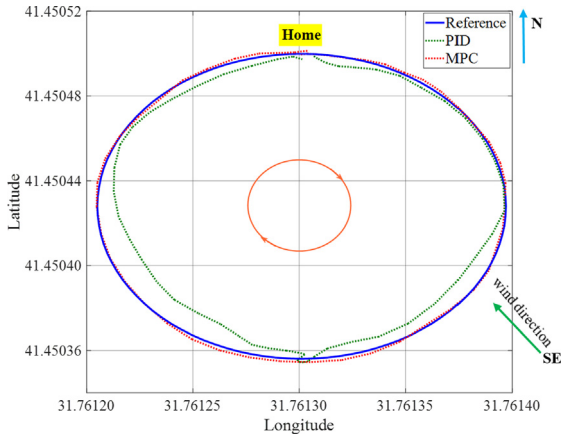

Fig. 23. MPC and PID performance of the three-axis gimbal for the second scenario.

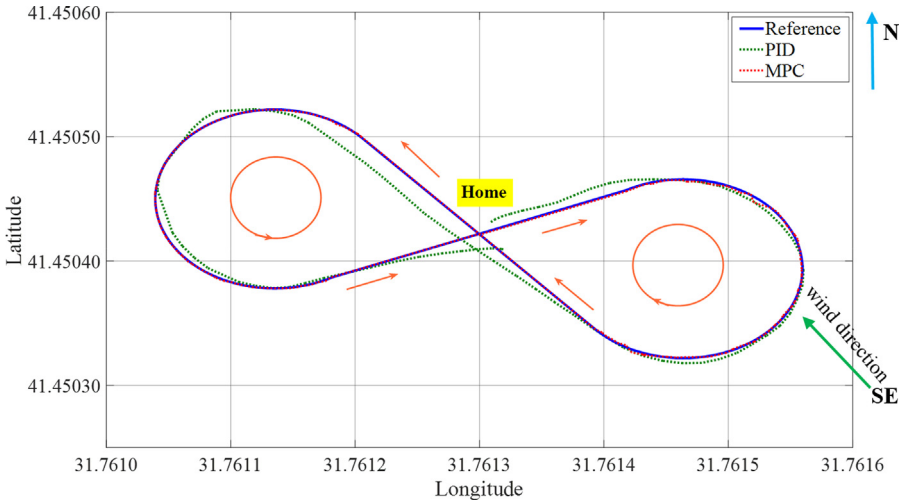

Fig. 24. MPC and PID performance of the three-axis gimbal for the third scenario.

Table 1
Controller performance comparison based on MSE values.

Scenario	Controller	MSE
1st	*PID*	1.766404
	MPC	0.033153
2nd	*PID*	1.840052
	MPC	0.032678
3rd	*PID*	1.061374
	MPC	0.014583

7. Conclusion

In this research, a novel MPC controller with the Hammerstein model has been proposed for the three-axis gimbal used in target tracking to be robust against external disturbance. The mathematical model of the three-axis gimbal system mounted on UAV under the external disturbance has been derived using the Lagrange equation. Simplified input–output model has been identified using nonlinear Hammerstein model structure as well as OE approach to show three-axis gimbal system nonlinearity. Then, the performance of proposed a novel MPC controller with Hammerstein model has been evaluated comparing with conventional PID controller in terms of robustness and quantitative study of error analysis. The stability and robustness of the three-axis gimbal system mounted on UAV controlled with the MPC algorithm has been tested different various mission scenarios. The MPC control with Hammerstein model of the three-axis gimbal system mounted on the UAV for target tracking under an external disturbance in real time was implemented by means of the DSP card on the autonomously moving UAV in which the developed algorithm has been embedded. This paper successfully illustrates the application of the MPC controller to control three-axis gimbal system mounted on UAV under external disturbances. The application of the MPC control unit with Hammerstein model to control the three-axis gimbal system mounted on UAV under external influences has been successfully illustrated in this paper. Considering the MPC performance, in future research activities, it will be focused that the collaborative control of the gimbal systems mounted on the multi-UAVs, which act as swarm, will be carried out in order to track a moving target in the air.

Acknowledgment

This study was supported by Zonguldak Bülent Ecevit University (BAP Project No: 2014-75737790-01). The authors would like to thank Zonguldak Bülent Ecevit University for their support.

Appendix A

PID controller is the most commonly used in control systems design to achieve the desired behaviors of different types of dynamic plants such as motor drives, magnetic and optic memories, industrial automation, instrumentation and robotics because of its simple and robust structure and performance. The PID controller is used to improve the dynamic response as well as to reduce or eliminate the steady-state error. The derivative controller adds a finite zero to the open-loop plant transfer function and improves the transient response. The integral controller adds a pole at the origin, thus increasing system type by one and reducing the steady-state error due to a step function to zero [46]. The output equation of the PID controller given the block structure in Fig. A.1 is

$$u(t) = K_P e(t) + K_I \int e(t)dt + K_D \frac{de(t)}{dt} \tag{A1}$$

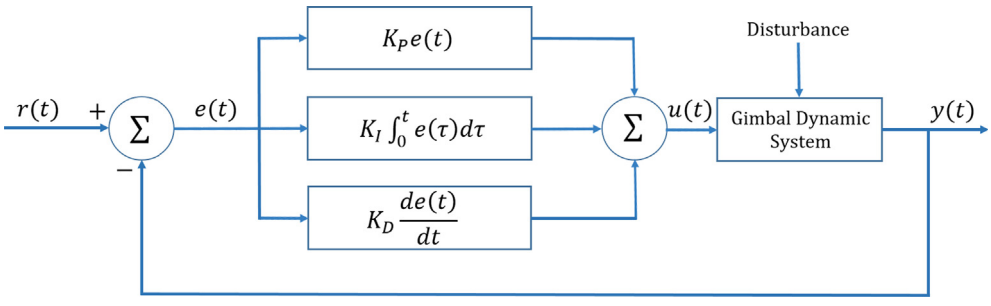

Fig. A1. PID controller block structure of three-axis gimbal system.

where K_P, K_I and K_D are proportional, integral and derivative gain terms of the PID controller, respectively, $e(t)$ represents the error caused by difference between reference and system response. The performance of the PID controller is determined by the K_P proportional parameter of the controller, the K_I integral control parameter and the K_D derivative control parameter [47]. In the study, conventional PID control of the three-axis gimbal system with mathematical model is realized to compensate for disturbances and uncertainties of the three-axis gimbal system mounted on UAV. In addition, the robustness of the conventional PID controller has been tested. The PID controller parameters are determined so that the closed-loop system meet the stability, robustness, transient response and steady-state accuracy. Note that all variables can be easily sampled by using appropriate frequency.

References

[1] G.V. Raffo, M.G. Ortega, F.R. Rubio, An integral predictive/nonlinear H∞ control structure for a quadrotor helicopter, Automatica 46 (1) (2010) 29–39.
[2] J. Liénard, A. Vogs, D. Gatziolis, N. Strigul, Embedded, real-time UAV control for improved, image-based 3D scene reconstruction, Measurement 81 (2016) 264–269.
[3] T. Tomic, K. Schmid, P. Lutz, A. Domel, M. Kassecker, E. Mair, I.L. Grixa, F. Ruess, M. Suppa, D. Burschka, Toward a fully autonomous UAV: research platform for indoor and outdoor urban search and rescue, IEEE Rob. Autom. Mag. 19 (3) (2012) 46–56.
[4] A. Altan, Ö. Aslan, and R. Hacıoğlu, "Model predictive control of load transporting system on unmanned aerial vehicle (UAV)," in Proc. Int. Conf. on Advances in Mech. and Robotics Eng. (AMRE), 2017, pp. 1-4.
[5] S. Siebert, J. Teizer, Mobile 3D mapping for surveying earthwork projects using an unmanned aerial vehicle (UAV) system, Autom. Constr. 41 (2014) 1–14.
[6] S.A. Quintero, J.P. Hespanha, Vision-based target tracking with a small UAV: optimization-based control strategies, Control Eng. Practice 32 (2014) 28–42.
[7] J. Zhou, Y. Li, J. Chen, L. Nian, H. Zhang, Research on six degrees of freedom compound control technology for improving photoelectric pod pointing accuracy, Opt. Rev. 24 (4) (2017) 579–589.
[8] X. Zhou, H. Zhang, R. Yu, Decoupling control for two-axis inertially stabilized platform based on an inverse system and internal model control, Mechatronics 24 (8) (2014) 1203–1213.
[9] H. Shraim, A. Awada, R. Youness, A survey on quadrotors: configurations, modeling and identification, control, collision avoidance, fault diagnosis and tolerant control, IEEE Aerospace Electron. Syst. Magazine 33 (7) (2018) 14–33.
[10] P.J. Kennedy, R.L. Kennedy, Direct versus indirect line of sight (LOS) stabilization, IEEE Trans. Control Syst. Tech. 11 (1) (2003) 3–15.
[11] J.M. Hilkert, Inertially stabilized platform technology concepts and principles, IEEE Control Syst. 28 (1) (2008) 26–46.
[12] M.M. Abdo, A.R. Vali, A.R. Toloei, M.R. Arvan, Stabilization loop of a two axes gimbal system using self-tuning PID type fuzzy controller, ISA Trans. 53 (2) (2014) 591–602.
[13] B. Li, D. Hullender, M. DiRenzo, Nonlinear induced disturbance rejection in inertial stabilization systems, IEEE Trans. Control Syst. Tech. 6 (3) (1998) 421–427.
[14] L. Edalati, A.K. Sedigh, M.A. Shooredeli, A. Moarefianpour, Adaptive fuzzy dynamic surface control of nonlinear systems with input saturation and time-varying output constraints, Mech. Syst. Signal Process. 100 (2018) 311–329.
[15] R. J. Rajesh and P. Kavitha, "Camera gimbal stabilization using conventional PID controller and evolutionary algorithms," in Proc. Int. Conf. on Computer, Communication and Control (IC4), 2015, pp. 1-6.
[16] H. Kouhi, M. Kabganian, F.F. Saberi, M. Shahravi, Robust control of a spin-stabilized spacecraft via a 1DoF gimbaled-thruster and two reaction wheels, ISA Trans. 66 (2017) 310–324.
[17] K.K. Tan, T.H. Lee, A. Mamun, M.W. Lee, C.J. Khoh, Composite control of a gyro mirror line-of-sight stabilization platform-design and auto-tuning, ISA Trans. 40 (2) (2001) 155–171.
[18] J.A.R. Krishnamoorty, R. Marathe, V.R. Sule, H∞ control law for line-of-sight stabilization for mobile land vehicles, Opt. Eng. 41 (11) (2002) 2935–2945.
[19] X. Lei, Y. Zou, F. Dong, A composite control method based on the adaptive RBFNN feedback control and the ESO for two-axis inertially stabilized platforms, ISA Trans. 59 (2015) 424–433.
[20] H. Taghavifar, S. Rakheja, Path-tracking of autonomous vehicles using a novel adaptive robust exponential-like-sliding-mode fuzzy type-2 neural network controller, Mech. Syst. Signal Process. 130 (2019) 41–55.
[21] W. Ji, Q. Li, B. Xu, D. Zhao, S. Fang, Adaptive fuzzy PID composite control with hysteresis-band switching for line of sight stabilization servo system, Aerospace Sci. Tech. 15 (1) (2011) 25–32.
[22] Y. Wang, X. Yang, H. Yan, Reliable fuzzy tracking control of near-space hypersonic vehicle using aperiodic measurement information, IEEE Trans. Ind. Electron. (2019).
[23] B.E. Demir, R. Bayir, F. Duran, Real-time trajectory tracking of an unmanned aerial vehicle using a self-tuning fuzzy proportional integral derivative controller, Int. J. Micro Air Vehicles 8 (4) (2016) 252–268.
[24] E. Skjong, S. A. Nundal, F. S. Leira, and T. A. Johansen, "Autonomous search and tracking of objects using model predictive control of unmanned aerial vehicle and gimbal: hardware-in-the-loop simulation of payload and avionics," in Proc. Int. Conf. on Unmanned Aircraft Systems (ICUAS), 2015, pp. 904-913.
[25] A.R. Toloei, M. Pirzadeh, A.R. Vali, Design of predictive control and evaluate the effects of flight dynamics on performance of one axis gimbal system, considering disturbance torques, Aerosp. Sci. Technol. 54 (2016) 143–150.
[26] X. Lei, P. Lu, The adaptive radial basis function neural network for small rotary-wing unmanned aircraft, IEEE Trans. Ind. Electron. 61 (9) (2014) 4808–4815.
[27] C.Y. Chang, Adaptive fuzzy controller of the overhead cranes with nonlinear disturbance, IEEE Trans. Ind. Inf. 3 (2) (2007) 164–172.
[28] M.K. Masten, Inertially stabilized platforms for optical imaging systems, IEEE Control Syst. 28 (1) (2008) 47–64.
[29] L. Ljung, System Identification Theory for User, Prentice-Hall, New Jersey, 1999.
[30] U. Forssell, L. Ljung, Identification of unstable systems using output error and Box-Jenkins model structures, IEEE Trans. Automatic Control 45 (1) (2000) 137–141.
[31] C.M. Cheng, X.J. Dong, Z.K. Peng, W.M. Zhang, G. Meng, Kautz basis expansion-based Hammerstein system identification through separable least squares method, Mech. Syst. Signal Process. 121 (2019) 929–941.
[32] R. Hacıoğlu, G.A. Williamson, Identification of wiener systems using reduced complexity Volterra models, IFAC Proc. 36 (16) (2003) 351–356.
[33] S. Karasu, A. Altan, Z. Saraç, R. Hacıoğlu, Estimation of fast varied wind speed based on NARX neural network by using curve fitting, Int. J. Energy Appl. Tech. 4 (3) (2017) 137–146.
[34] E.W. Bai, D. Li, Convergence of the iterative Hammerstein system identification algorithm, IEEE Trans. Automatic Control 49 (11) (2004) 1929–1940.
[35] F. Ding, X.P. Liu, G. Liu, Identification methods for Hammerstein nonlinear systems, Digital Signal Process. 21 (2) (2011) 215–238.
[36] A. Wills, T.B. Schön, L. Ljung, B. Ninness, Identification of Hammerstein-Wiener models, Automatica 49 (1) (2013) 70–81.
[37] S.M. Kay, Fundamentals of Statistical Signal Processing, Prentice Hall PTR, 1993.
[38] E.F. Camacho, C. Bordons, Model Predictive Control, Springer Science & Business Media, London, 2007.

[39] F. Gavilan, R. Vazquez, E.F. Camacho, "An iterative model predictive control algorithm for UAV guidance, IEEE Trans. Aerospace Electron. Syst. 51 (3) (2015) 2406–2419.
[40] H. Guo, D. Cao, H. Chen, Z. Sun, Y. Hu, Model predictive path following control for autonomous cars considering a measurable disturbance: Implementation, testing, and verification, Mech. Syst. Signal Process. 118 (2019) 41–60.
[41] H. Guo, C. Shen, H. Zhang, H. Chen, R. Jia, Simultaneous trajectory planning and tracking using an MPC method for cyber-physical systems: A case study of obstacle avoidance for an intelligent vehicle, IEEE Trans. Ind. Inf. 14 (9) (2018) 4273–4283.
[42] H. Guo, H. Chen, F. Xu, F. Wang, G. Lu, Implementation of EKF for vehicle velocities estimation on FPGA, IEEE Trans. Ind. Electron. 60 (9) (2012) 3823–3835.
[43] F. Xu, H. Chen, X. Gong, Q. Mei, Fast nonlinear model predictive control on FPGA using particle swarm optimization, IEEE Trans. Ind. Electron. 63 (1) (2015) 310–321.
[44] L. Guo, B. Gao, Q. Liu, J. Tang, H. Chen, On-line optimal control of the gearshift command for multispeed electric vehicles, IEEE/ASME Trans. Mechatron. 22 (4) (2017) 1519–1530.
[45] [Online].Available: http://www.ti.com/lit/ds/symlink/tms320f28232.pdf.
[46] Y. Li, K.H. Ang, G.C. Chong, PID control system analysis and design, IEEE Control Syst. 26 (1) (2006) 32–41.
[47] H. Feng, C.B. Yin, W.W. Weng, W. Ma, J.J. Zhou, W.H. Jia, Z.L. Zhang, Robotic excavator trajectory control using an improved GA based PID controller, Mech. Syst. Signal Process. 105 (2018) 153–168.

Aytaç Altan recieved his B.Sc. and M.Sc. degrees in the department of Electrical Electronics Engineering from Anadolu University in 2004 and 2006, respectively. He is received his Ph.D. degree in the department of Electrical Electronics Engineering from Zonguldak Bülent Ecevit University in 2018. He is currently a lecturer at the department of Electrical Electronics Engineering at the Zonguldak Bülent Ecevit University in Turkey. His research interests include system identification, signal processing, image processing, model based control and robotic systems.

Rıfat Hacıoğlu received his B.Sc. degree in the department of Electrical Electronics Engineering from Dokuz Eylül University in 1993. He is received his M.Sc. and Ph.D., degrees in the department of Electrical and Computer Engineering from Illinois Institute of Technology, Chicago, USA, in 1996 and 2002, respectively. He is currently an Associate Professor at the department of Electrical Electronics Engineering at the Zonguldak Bülent Ecevit University in Turkey. His research interests are signal processing, control applications, linear and nonlinear system identification, parametric model estimation approaches, microprocessor based control systems, image identification problems.